ON THE IONIC CHEMISTRY IN DC COLD PLASMAS OF H_2 WITH Ar

I. Méndez, I. Tanarro*, V. J. Herrero

Instituto de Estructura de la Materia, CSIC, Serrano 123, 28006 Madrid, Spain

*Corresponding author: itanarro@iem.cfmac.csic.es

Abstract

An experimental diagnosis and kinetic modeling of the ionic chemistry in low pressure DC plasmas of H_2/Ar has been carried out. The studies were performed at pressures of 2 Pa and 0.7 Pa, in a hollow-cathode discharge reactor, using as plasma precursor a H_2/Ar mixture with 15% Ar content. Experimental measurements include distributions of ion fluxes to the cathode, as well as electronic temperatures and densities in the plasma glow. Besides the species resulting directly from electron impact ionization (H^+, H_2^+, Ar^+ and Ar^{2+}), the ions H_3^+ and ArH^+ were found to be formed in large amounts through protonation reactions in the glow. In spite of the not too large variation in the pressure of the two plasmas, the differences in the ion distributions are worth mentioning. In the 2 Pa discharge (but not in the 0.7 Pa), H_3^+ was the dominant ion and ArH^+ exceeded markedly the Ar^+ signal. On the other hand, the appearance of Ar^{2+} in the two plasmas points at the relevance of high energy electrons. The experimental results can be accounted for by a simple kinetic model, after including corrections for the presence of a small fraction (< 3%) of high energy (> 50 V) electrons and for the attenuation of the Ar^+ ions in the sheath through asymmetric charge exchange with H_2.

1. Introduction

Ar/H_2 plasmas find widespread application in diverse fields of material science, where they are employed for deposition and sputtering[1-5] or as particle sources. [6-9] In conjunction with optical emission spectroscopy and mass spectrometric techniques, they are also widely used for elemental analysis (see ref. 10-18 and references cited therein), where the addition of H_2 to Ar glow discharges has been found to enhance in many cases the sputtering yields and has led often to improvements in the sensitivity and detection limits.

Models of varying complexity[5,7,19-23] have been applied to these systems in an attempt to elucidate the fundamental mechanisms and the role of the reactive species involved in their chemistry. Some issues like the decrease in H_2 dissociation, the anomalous loss of ionization, the influence of metastable atoms, or the distinct role of electrons with different kinetic energy have deserved special attention. In spite of the progress achieved over the last decades, doubts and controversies still persist. As an example, the mentioned loss of ionization has been variously attributed to dissociative ion electron recombination[6,22] or to the quenching by H_2 of the metastable Ar* atoms acting as ion precursors.[24] Although the same fundamental physicochemical processes are always involved, their relative weight in the overall chemistry may be very different and the peculiarities of each case should be carefully considered.

Most studies of Ar/H_2 plasmas have been focused on mixtures with small H_2 proportions that mimic conditions most commonly found in the discharges used for practical applications. In the present work, which addresses the plasma ion chemistry from a basic point of view, we use a complementary approach and investigate Ar/H_2 mixtures dominated by H_2. We can thus take advantage of our previous study on H_2 DC glow discharges,[25] which is here extended by preparing a precursor H_2/Ar mixture with a 15% of Ar. In this way, we can observe the modifications induced by Ar in our well characterized H_2 plasma. The experiments are carried out in a hollow cathode (DC) reactor. Hollow cathode discharges provide a useful means for the study of elementary processes in low pressure plasmas. In particular, they allow an easy control of the size and shape of the discharge and provide an enlarged negative glow region with a very small electric field and relatively homogeneous properties.

Electron temperatures and densities, as well as mass spectra of the ions present in the plasma, are recorded for different discharge conditions, and a simple chemical model is used

to rationalize the measured data. The basic mechanisms leading to the observed ion distributions are identified and discussed. Special emphasis is laid on the role of high energy electrons and on the influence of sheath collisions on the ion fluxes reaching the cathode wall.

2 Experimental section

The experimental plasma reactor has been described in previous works.[25,26] It consists of a grounded cylindrical stainless steel vessel (10 cm diameter, 34 cm length), and a central anode. The whole system can be pumped to a background pressure of 10^{-6} mbar by a 450 l/s turbomolecular pump and a rotary pump. The vessel walls have different ports for connection of gas inlets, diagnostics tools, observation windows and pressure gauges. The pressure was controlled by balancing the gas flow with a needle valve at the entrance and a butterfly valve at the exit of the reactor. Mixtures of H_2/Ar (15%) were used as discharge precursors. The pressures of study were 2 Pa and 0.7 Pa, as measured with a capacitance manometer. Typical residence times of the gases in the reaction chamber were ≈ 0.5 - 1 s.

Plasma currents I_p ~ 150 mA and supply voltages V ~ 500 and 350 V were used in the 2 Pa and 0.7 Pa discharges, respectively. In order to initiate the discharges, an electron gun built in our laboratory, consisting basically of a tungsten filament operating at 2 A and –2000 V_{DC}, was employed.

A Plasma Process Monitor, Balzers PPM421, was used for the detection of both neutrals and ions from the plasma. It consists of an electron bombardment ionizer, an electrostatic focusing system, a cylindrical mirror ion energy analyser and a quadrupole mass filter, with a secondary electron multiplier in the counting mode. For the detection of ions, the electron bombardment ionizer is switched off and the ions are allowed to enter the detector directly from the plasma. The apparatus was installed in a differentially pumped chamber connected to the reactor through a 100 μm diaphragm. During operation, the pressure in the detection chamber was kept in the 10^{-7} mbar range by means of a 150 l/s turbomolecular pump and a dry pump.

Ion fluxes were calculated by integrating the ion energy distributions recorded in the experiments for each individual mass value. For the pressures involved, these energy distributions consist mainly in a narrow and sharp peak for each ion, located close to the anode-cathode potential.[27,28] The sensitivity of the plasma monitor to the masses of the

different ions, which depends among other factors on the multiplier condition, was calibrated for singly charged ions over the range of interest.[25,29] The sensitivity for the higher mass ions (Ar^+, ArH^+), at m/q=40 and 41 was found to be roughly one half of that for m/q=4, and no appreciable mass dependence was found below between m/q= 2 and 4. For m/q=1, at the edge of the mass filter, the sensitivity was again lower, approximately one third of the value corresponding to m/q= 2-4. A comparison with Faraday cup measurements showed that the gain of the electron multiplier for doubly charged Ar^{2+} ions (m/q=20) was larger than that of Ar^+ by a factor of two for the multiplier voltage of 2800 V used in the experiments. This result is in accordance with similar measurements by other authors.[30]

The electron mean temperature, T_e, and total charge density, n_e, in the cylindrical reactor were measured by means of a double Langmuir probe built in our laboratory[31] by assuming a collision free probe sheath and orbital limited motion.[32] To estimate total charge densities from the characteristic curves of the Langmuir probe, a mean ion mass was used in each case, weighted according to the ion density distributions deduced from the measurements of the Plasma Process Monitor. It is also tacitly assumed that negative ions are negligible in the plasmas studied and that electroneutrality is brought about by a balance between the density of electrons and that of positive ions.

3 Results and Discussion

A summary of the experimental results for the two discharges investigated is given in Table 1. The electronic temperatures (2.5 and 3.5 eV) measured in the Ar/H_2 plasma are lower, roughly by a factor of two, than those obtained previously in the same reactor for a pure H_2 plasma at the same pressures.[25] The presence of the Ar atoms, even in moderate proportion, leads thus to a more efficient energy transfer of the initial kinetic energy of the electrons to the heavier species in the plasma.

The ion fluxes reaching the cathode are also included in Table 1, and have been represented in Fig. 1 and 2. In each case, the sum of all ion fluxes has been normalized to 1. Signals with m/q ratios 1, 2, 3, 20, 40 and 41, corresponding respectively to the ions H^+, H_2^+, H_3^+, Ar^{2+}, Ar^+ and ArH^+, were detected in the two discharges. Under the low pressure conditions of our experiments, no trace of Ar_2^+ (m/q =80), a species formed in ternary collisions, was observed. The two distributions are dominated, as expected, by the light

hydrogenic ions (masses 1-3), which are generated from the most abundant precursor and leave the plasma more swiftly.

			Normalized Ion Fluxes					
Pressure (Pa)	T_e (eV)	n_e (cm^{-3})	H^+	H_2^+	H_3^+	Ar^{++}	Ar^+	ArH^+
2.0 ± 0.1	2.5	$3.6 \cdot 10^{10}$	0.24	0.16	0.52	0.013	0.008	0.066
0.7 ± 0.1	3.5	$2.3 \cdot 10^{10}$	0.14	0.39	0.35	0.01	0.027	0.075

Table 1. Experimental results for the two H_2 + Ar (15%) discharges investigated, at 2 and 0.7 Pa. The relative errors in electron temperatures and densities, deduced from the characteristic curves of the Langmuir probe, are ≈ 30%; and the relative errors in the normalized ion fluxes, deduced from the experimental dispersion of data in a set of four consecutive measurements, are ≈ 10%.

The pressure decrease from 2 to 0.7 Pa leads to a pronounced change in the ion flux distribution. At the lower pressure, the major ions are H_2^+ and H_3^+ (in that order), which are present in comparable amounts, and the flux of ArH^+ is larger than that of Ar^+ by a factor of about two. At the higher pressure, H_3^+ is neatly the dominant ion, and the relative flux of Ar^+ is smaller by an order of magnitude than that of ArH^+. In the two discharges there is a small, but appreciable, Ar^{2+} flux.

For the rationalization of the experimental results, we have extended the simple zero order kinetic model previously applied to discharges of pure H_2.[25] The model is based on the numerical integration of a system of coupled differential equations, which account for the time evolution of the plasma species, from the ignition point, to the attainment of the steady state. It uses as input parameters the experimental pressures and gas flows, and also the measured electronic temperatures and densities, T_e and n_e, which are assumed to be homogeneously distributed throughout the plasma volume V_p. This volume is estimated to be cylindrical and coincident with that of the negative glow region, which is separated from the metallic walls of the chamber (cathode) by the plasma sheath, with an estimated width of 1.5-2 cm for the conditions of our reactor.[28] It is further assumed that the ion temperature in the glow (T_{ion}) is equal to the gas temperature (T_{gas} =300 K). The concentration of the various

plasma species is supposed to be controlled in principle by the set of homogeneous and heterogeneous reactions listed in the first column of Tables 2 and 3.

Homogeneous Reactions	k^A	k^B
1.- $H + e \rightarrow H^+ + 2e$	$6.50 \times 10^{-9} \times T_e^{0.49} \times e^{-12.89/Te}$ (25)	4.2×10^{-8} (42)
2.- $H_2 + e \rightarrow H^+ + H + 2e$	$3.00 \times 10^{-8} \times T_e^{0.44} \times e^{-37.73/Te}$ (25)	4.5×10^{-9} (42)
3.- $H_2^+ + e \rightarrow H^+ + H + e$	$1.07 \times 10^{-7} \times T_e^{0.049} \times e^{-9.69/Te}$ (25)	
4.- $H_2^+ + e \rightarrow H^+ + H^+ + 2e$	$2.12 \times 10^{-9} \times T_e^{0.31} \times e^{-23.30/Te}$ (25)	
5.- $H_2^+ + H \rightarrow H_2 + H^+$	6.4×10^{-10} (33)	
6.- $H_2 + H^+ \rightarrow H_2^+ + H$	1.19×10^{-22} (25)	
7.- $H_2 + e \rightarrow H_2^+ + 2e$	$3.12 \times 10^{-8} \times T_e^{0.17} \times e^{-20.08/Te}$ (25)	5.0×10^{-8} (42)
8.- $H_3^+ + e \rightarrow H_2^+ + H + e$	$4.85 \times 10^{-7} \times T_e^{-0.05} \times e^{-19.17/Te}$ (25)	
9.- $H_2^+ + e \rightarrow H^* + H$	$a + b \times T_e + c \times T_e^2 + d \times T_e^3 + e \times T_e^4$ (25)	
10.- $H_2^+ + H_2 \rightarrow H_3^+ + H$	2.0×10^{-9} (33)	
11.- $H_3^+ + e \rightarrow 3\ H$	$0.5 \times K^{(**)}$ (25)	
12.- $H_3^+ + e \rightarrow H_2 + H$	$0.5 \times K^{(**)}$ (25)	
13.- $H_2 + e \rightarrow 2\ H + e$	$1.75 \times 10^{-7} \times T_e^{-1.24} \times e^{-12.59/Te}$ (25)	1×10^{-8} (42)
14.-$Ar + e \rightarrow Ar^+ + 2e$	$2.53 \times 10^{-8} \times T_e^{0.5} \times e^{-16.3/Te}$ (34)	1.6×10^{-7}(34)
15.-$Ar + e \rightarrow Ar^{++} + 3e$	$2.58 \times 10^{-9} \times T_e^{0.5} \times e^{-47/Te}$ (34)	1.1×10^{-8} (34)
16.-$Ar^+ + e \rightarrow Ar^{++} + 2e$	$1.9 \times 10^{-8} \times T_e^{0.5} \times e^{-27.7/Te}$ (39)	
17.-$H_2^+ + Ar \rightarrow ArH^+ + H$	2.1×10^{-9} (33)	
18.-$H_3^+ + Ar \rightarrow ArH^+ + H_2$	3.65×10^{-10} (33)	
19.-$Ar^+ + H_2 \rightarrow H_2^+ + Ar$	$0.02 \times 8.9 \times 10^{-10}$ (33)	
20.-$Ar^+ + H_2 \rightarrow ArH^+ + H$	$0.98 \times 8.9 \times 10^{-10}$ (33)	
21.-$ArH^+ + H_2 \rightarrow H_3^+ + Ar$	6.3×10^{-10} (33)	

(*) $a = 7.51 \times 10^{-9}$, $b = -1.12 \times 10^{-9}$, $c = 1.03 \times 10^{-10}$, $d = -4.15 \times 10^{-12}$, $e = 5.86 \times 10^{-14}$
(**) $K = 8.39 \times 10^{-9} + 3.02 \times 10^{-9} \times T_e - 3.80 \times 10^{-10} \times T_e^2 + 1.31 \times 10^{-11} \times T_e^3 + 2.42 \times 10^{-13} \times T_e^4 - 2.30 \times 10^{-14} \times T_e^5 + 3.55 \times 10^{-16} \times T_e^6$

Table 2. Homogeneous reactions considered. Rate coefficients, k, are given in cm^3s^{-1}. k^A: Rate coefficients for Maxwellian electrons at T_e (in eV). k^B: Rate coefficients for high energy

electrons (see text). Numbers in parentheses indicate the references used as sources for the corresponding rate coefficients.

Heterogeneous Reactions	Wall Reaction Probabilities
1.- $H + Wall \rightarrow H_2$	$\gamma = 0.03$
2.- $H^+ + Wall \rightarrow H$	$\gamma = 1$
3.- $H_3^+ + Wall \rightarrow H_2 + H$	$\gamma = 1$
5.-$Ar^+ + Wall \rightarrow Ar$	$\gamma = 1$
6.-$ArH^+ + Wall \rightarrow Ar + H$	$\gamma = 1$
7.-$Ar^{++} + Wall \rightarrow Ar$	$\gamma = 1$

Table 3. Heterogeneous reactions considered

Two improvements have been introduced in the treatment of the hydrogenic species: a) A differential equation, describing the behavior of H^+ has been added. In our previous work,[25] the concentration of this ion was obtained from the electroneutrality condition. Consequently, to avoid inconsistencies in our simple model, it was necessary to change the gamma coefficients for ions neutralization in the walls from 0.9[25] to 1, to guarantee that so many charges as produced in the glow do disappear in the walls. b) The rate coefficients for the reactions $H_2 + H_2^+ \rightarrow H_3^+ + H$ and $H_2^+ + H \rightarrow H_2 + H^+$ have now been changed to $k = 2 \times 10^{-9}$ cm^3 s^{-1} and 6.4×10^{-10} cm^3 s^{-1} respectively, which correspond to the generally accepted rate constants from ref. 33. The previous results on pure H_2 plasmas have been verified after the introduction of the new differential equation and the new rate coefficients, which are somewhat smaller than those used in ref. 25 (see second column of Table 2). Calculations with these new improvements lead only to small changes that do not modify the former conclusions.

Electron impact ionization rate coefficients for the production of Ar^+ and Ar^{2+} have been calculated by fitting the up-going post-threshold part of the measured cross sections[34] to

a line-of-centers functionality[35] (sometimes termed an Arrhenius-like cross section functionality), and by assuming a Maxwellian velocity distribution for electrons in the plasma, and are also indicated in the second column of Table 2. Ion molecule reactions for Ar containing ions have been taken from the literature sources indicated in Table 2. The dissociative electron recombination of $ArH^+ + e \rightarrow Ar + H$ has not been included in the model. This process, with an assumed rate coefficient of the order of 10^{-7} cm^3 s^{-1}, had been considered in some works to be at the root of the loss of ionization observed in different Ar/H_2 discharges,[6,7,22] however, recent measurements[36] have produced rate coefficients smaller than 1×10^{-8} cm^3 s^{-1} for collision energies below 35 eV, and of the order of 10^{-10} cm^3 s^{-1} for thermal energies, demonstrating that this process is usually unimportant in glow discharges.[23] The dissociative recombination of the hydrogenic ions has larger rate coefficients. In particular, that of H_3^+, of special interest in astrophysics, has been the subject of a long standing controversy (see ref. 37and references therein). Current studies[37] indicate that the rate coefficient is indeed of the order of 10^{-7} cm^3 s^{-1} for the low collision energies typical of interstellar space, but drops to values in the 10^{-8}-10^{-9} cm^3 s^{-1} range for the electron energies of relevance in the present plasmas. Although the electron recombination of H_3^+ has been kept in the model for completion, it turns out to be practically negligible, as discussed in ref. 25. Under the present experimental conditions, with low pressures, and electron densities of the order of 10^{10} cm^{-3}, the fate of virtually all ions generated in the glow is diffusion to the cathode sheath, followed by wall recombination. It should be also noted that the model does not include excited species or atoms and ions sputtered from the metallic walls of the reactor.

The calculated concentrations of ionic species in the negative glow are transformed into relative ion fluxes multiplying by a factor $(q_i/m_i)^{0.5}$ and are compared with the experimental results in Fig. 1a and 2a. The predicted ion fluxes bear some similitude for the two pressures. Although the appearance of large amounts of H_3^+ and ArH^+ is reproduced in the model calculations and can be traced back chiefly to the efficient protonation reactions of Table 2, there are striking differences with the experimental values. In both cases, H_3^+ is predicted to be by far the dominant plasma ion, and the H_2^+ signals are much lower than the measured values. Moreover, the model leads to a negligible amount of Ar^{2+} in the plasma (some two orders of magnitude lower that those of Ar^+). The experimental results, in particular the appearance of Ar^{2+} and the H_3^+/H_2^+ ratios, cannot be reproduced by changing the T_e values within their experimental uncertainties, indicated in Table 1.

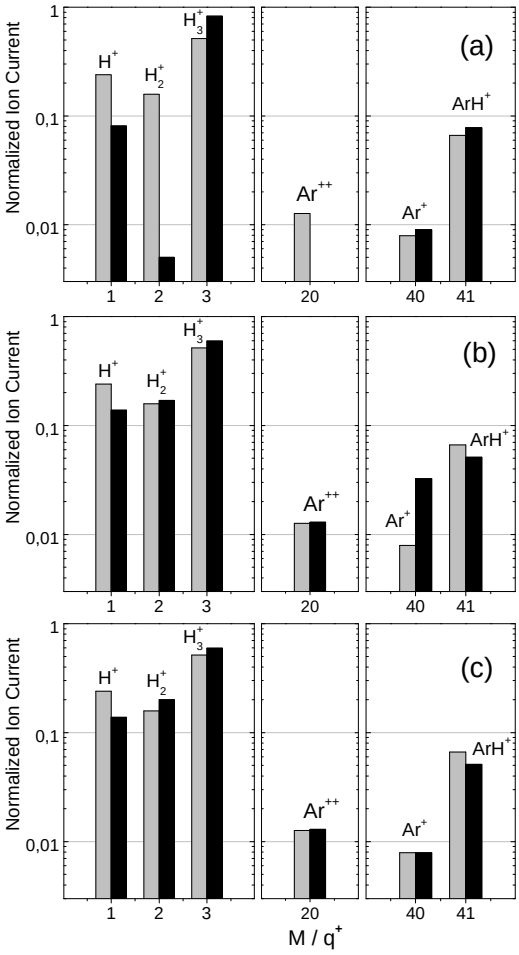

Fig. 1. All panels, grey bars: Measured fluxes (normalized to one) of the ions reaching the cathode in a hollow cathode DC discharge of H_2/Ar(15%) for a pressure of 2 Pa. Fig. 1a, black bars: Ion fluxes calculated with the model with $n_e = 3.6 \times 10^{10}$ cm^{-3}, and taking only into account the Maxwellian electrons at $T_e = 2.5$ eV, deduced from the double Langmuir probe; without attenuation of Ar^+ in the sheath (see text). Fig. 1b, black bars: Ion fluxes calculated with the model with 0.7% high energy electrons (see text) and without Ar^+ attenuation in the sheath. Fig. 1c black bars: Ion fluxes calculated with the model for 0.7 % high energy electrons and with attenuation of the Ar^+ flux in the sheath (eqn (1)).

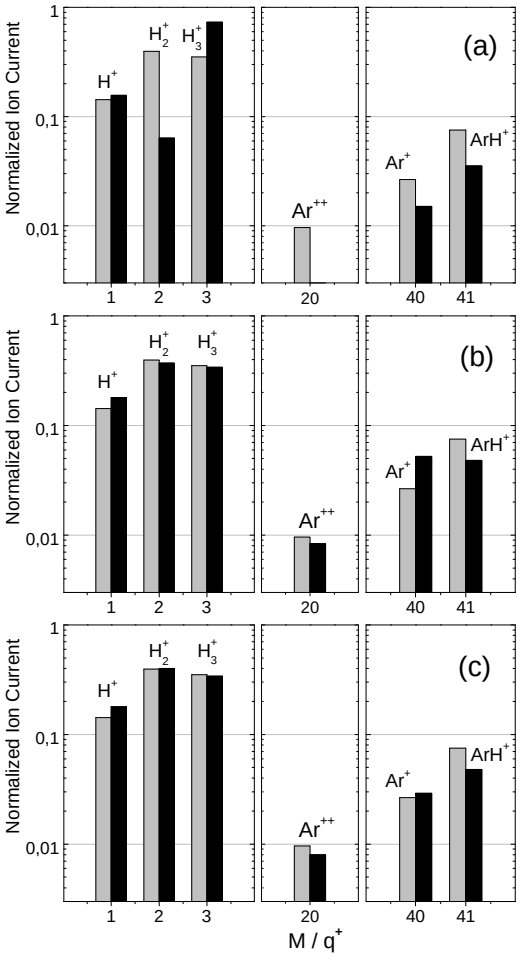

Fig. 2. Same as Fig. 1, but for a pressure of 0.7 Pa, $n_e = 2.3 \times 10^{10}$ cm^{-3} and $T_e = 3.5$ eV. In this case, the fraction of high energy electrons used in the calculations of the two lower panels (Fig. 2b and 2c) is 2.3%.

The virtual absence of Ar^{2+} in the model predictions of Fig. 1a and 1b suggests that high energy electrons are not accounted for properly. In fact, electron impact ionization of Ar (reaction 15), with a threshold of ≈ 48 eV,[34] is the main source of Ar^{2+} in this type of plasmas.[38] The other Ar^{2+} source included in the model, namely, electron impact ionization of Ar^+ (reaction 16) has indeed a lower threshold and a larger cross section,[39] but its contribution to the global production of Ar^{2+} is very small, given the low ionic concentrations in the plasma (the concentration of Ar^+ ions is typically more than five orders of magnitude lower than that of Ar atoms).

The amount of electrons with energies beyond the threshold of reaction 15 is almost negligible in the Maxwellian velocity distributions used in the calculations, which correspond to the measured electron temperatures (T_e < 4 eV). Nevertheless, the presence of high energy electrons in DC glow discharges is well documented both in experiments[40] and in accurate self-consistent plasma models.[41] If this high energy component is small enough, it will not be discerned in the Langmuir probe measurements used for the determination of T_e, which are relatively insensitive to the detailed shape of the electron energy distribution. We will now introduce an empirical correction to the model, in order to consider approximately the effects of these high energy electrons. We will assume that the free electrons in the plasma are divided into two groups. The first of these groups, with a Maxwellian energy distribution corresponding to the measured T_e values, and the second group, with energies between ≈ 50 V and the energy of the voltage fall in the sheath (≈ 500 V for 0.7 Pa and ≈ 350 V for 2 Pa). Over this energy range, the rate coefficients, $k = \sigma \times v$, where σ is the relevant cross section and *v*, the corresponding electron velocity for electron impact processes, do not change much, since the post maximum decline of the cross sections with growing energy[34,39,42] is approximately compensated by the corresponding increase in *v*. Taking this into account, we will further assume that dissociating and ionizing collisions of this higher energy electron group with atoms and molecules are characterized by a rate coefficient: $k = \langle \sigma \times v \rangle$, where the average extends over the 70-350 eV interval. These ionization and dissociation rate coefficients, calculated with the cross sections of ref. 34 and 42 are listed in the third column of Table 2. Rate coefficients for ion-electron processes are not included, since they have proved irrelevant, given the low concentration of the charged species. For the dissociation of H_2 (reaction 13), no data were found beyond 90 eV[42] and we have taken the $\sigma \times v$ product corresponding to 80 eV. The ratio of high energy to low energy (Maxwellian at T_e) electrons can be now estimated by varying the relative weight of their respective rate coefficients (second and third columns of Table 2) in the model.

Fig. 3a,b shows the calculated plasma ion concentrations as a function of the fraction of high energy electrons for 2 and 0.7 Pa respectively. The ion concentrations predicted for 0% high energy electrons correspond to the ion currents shown in Fig. 1a and 2a, which were commented on in the previous paragraphs. The ion distributions leading to a best agreement with the experimental measurements are singled out in Fig. 3a,b with rectangles for the two pressures investigated. The corresponding ion fluxes are shown in Fig. 1b and 2b.

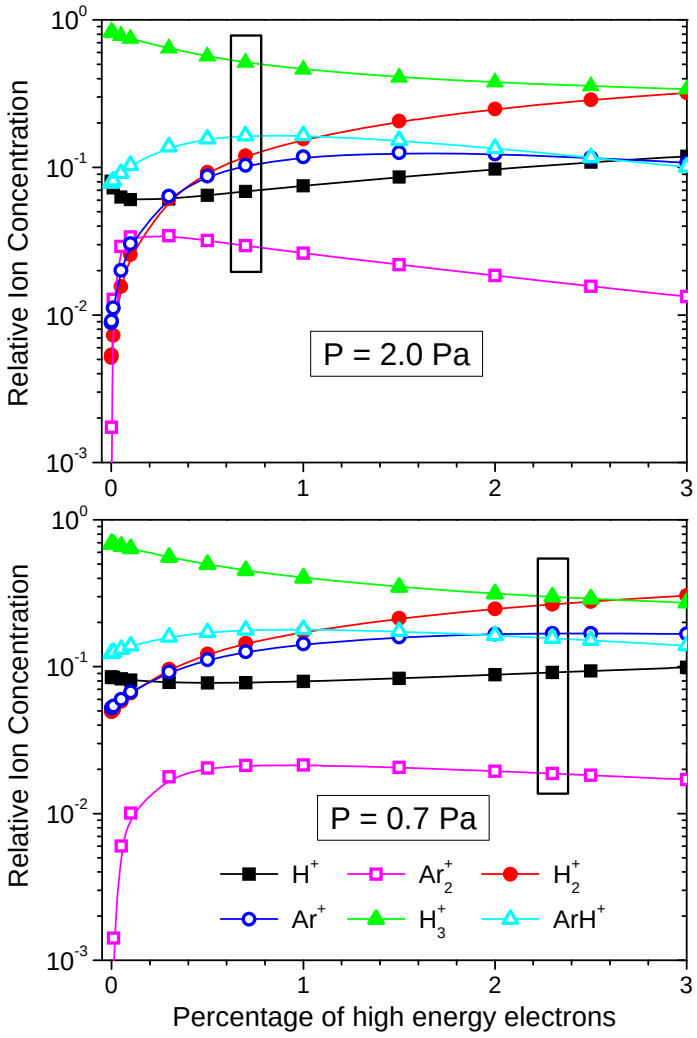

Fig. 3 Calculated relative ion concentrations in the glow of H_2/Ar (15%) DC discharges, as a function of the fraction of high energy electrons (see text). Upper panel, for a pressure of 2 Pa. Lower panel, for a pressure of 0.7 Pa. The rectangles in the graphs correspond to the fractions giving best agreement with experiment.

Inspection of Fig. 3 shows that a very small amount of fast electrons (even less than 0.2%) is enough to justify concentrations of Ar^{2+} ions like those measured in the experiments, and do not vary much afterwards. Moreover, a significant variation of the H_2^+/H_3^+ ratio is also observed in the figure. With growing proportion of high energy electrons, the number of H_2^+ ions produced by electron impact increases faster than that of the H_3^+ ions generated through reaction 10. The ion distributions leading to a best accord with the experiments correspond to small fractions of high energy electrons, 0.7% for 2.0 Pa and 2.3% for 0.7 Pa, too small to be

detectable in the comparatively coarse Langmuir-probe measurements. The decrease of the fraction of high energy electrons with growing pressure is consistent with intuitive expectations of a more efficient electron thermalization. The comparison of calculated and experimental ion flux values (Fig. 1b and 2b) shows that the introduction of high energy electrons is not only necessary for the explanation of the appearance of Ar^{2+}, but also for a proper description of the distribution of the predominant H_x^+ ions. In particular, the presence of high energy electrons increases the value of the effective rate coefficient for reaction 7 and leads to a marked growth in the relative concentration of H_2^+, bringing the results of the calculations in much better agreement with experiment.

As mentioned above, at 0.7 Pa, H_2^+ is the major plasma ion, its concentration slightly exceeding that of H_3^+. At 2 Pa, with a smaller proportion of high energy electrons and a larger collision frequency, H_3^+ is prevalent. An analogous change in the H_x^+ distribution was observed in a previous work on pure H_2 plasmas,[25] carried out in the same reactor, and the experimental results could be reproduced with the same kinetic model without invoking the presence of a distinct group of high energy electrons. However, in the pure hydrogen plasmas, the measured electron temperatures were a factor of two higher for the same pressures, and the corresponding electron impact rate coefficients for "Maxwellian" electrons at T_e (the equivalent to the second column of table 2) were significantly larger than in the present case. Under these circumstances, the likely contribution of a small fraction of high energy electrons to the effective electron impact rate coefficients should be appreciably smaller.

In spite of the improvement described in the previous paragraph, the introduction of high energy electrons in the model cannot account for the ratio of the observed fluxes of Ar^+ and ArH^+, and, in particular, for the pronounced decrease in the number of Ar^+ ions detected with growing pressure. Since the relevant sources of Ar^+ and its sinks at the roughly thermal collision energies of the glow are already included in the model, we must consider additional processes than can interfere selectively with the detection of Ar^+ in the mass spectrometer. In fact ions leaving the glow are accelerated in the sheath to several hundred eV before reaching the cathode wall, where they are sampled and detected by the mass spectrometer. For these ion energies, asymmetric charge exchange of Ar^+ with H_2 molecules, the most abundant gas species, can lead to a significant attenuation of the Ar^+ signal. The evolution of the cross sections with collision energy for reaction of Ar^+ with H_2 leading to asymmetric charge exchange (reaction 19) and chemical exchange (reaction 20) is represented in Fig. 4.

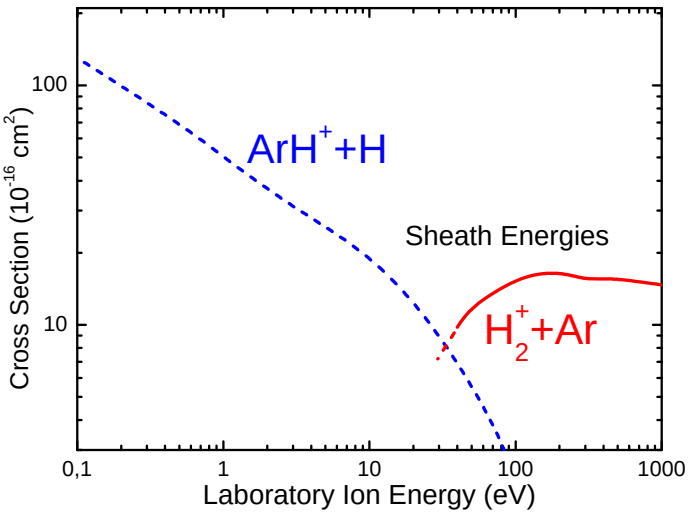

Fig. 4 Cross sections for collisions of Ar^+ ions with H_2 as a function of ion energy. Dashed line, proton exchange[43] ($Ar^+ + H_2 \rightarrow ArH^+ + H$). Solid line: asymmetric charge exchange[48] ($Ar^+ + H_2 \rightarrow H_2^+ + Ar$). The range of ion energies in the sheath is also indicated in the figure. The thermal ion-molecule collision energies within the glow correspond to laboratory ion energies of ≈ 0.8 eV (see Fig. 7 of ref. 43).

As can be seen, at low energies the proton exchange reaction prevails,[43] but the charge exchange channel is predominant for ion energies above 30 eV and has an appreciable cross section (≈ 1.5 x 10^{-15} cm^2) over most of the energy range relevant for sheath collisions (up to 350-500 V). For the rest of the ions in the plasma (H^+, H_2^+, H_3^+, ArH^+, and Ar^{2+}), there are no efficient collisional loss mechanisms in the sheath under the conditions of the present experiments.[22,44-47] The largest cross sections correspond to symmetric charge exchange of Ar^+ and H_2^+, but these processes lead to a modification of the ion energy distribution[28] rather than to a neat ion loss. Given the high accelerating voltage in the sheath, the low thermal velocity spread in the glow, and the small angle of admittance of the 100 μm orifice at the entrance of the mass spectrometer, we can assume that most of the detected ions will cover the distance between the plasma edge and the sampling orifice in a straight line trajectory, roughly perpendicular to the cathode wall, i.e. they will follow the shortest way, which corresponds to the sheath width. With these assumptions the attenuation of Ar^+ in the sheath can be taken into account approximately by assuming a Lambert-Beer attenuation:

$$I = I_0 \exp\left(-n_{H_2} d_s \sigma_a\right) \quad (1)$$

where I is the measured signal, I_0 the un-attenuated intensity, n_{H_2} the density of molecular hydrogen, d_s the sheath width, and σ_a the cross section for asymmetric charge exchange. Taking[28] $d_s \approx 2$ cm and $\sigma_a \approx 1.5 \times 10^{-15}$ cm^2,[44,48] the (I_0/I) ratio is 1.78 for a pressure of 0.7 Pa and 4.20 for a pressure of 2 Pa. We can now use these values to correct the calculated Ar^+ signals. To a first approximation, the attenuation of Ar^+ ions is paralleled by a corresponding increase in the concentration of H_2^+ that must also be taken into account. The calculated ion flux distributions corrected with the effects of asymmetric charge exchange of Ar^+ are displayed in Fig. 1c and 2c respectively. As can be seen, the strong attenuation of the Ar^+ ion, whose measured flux is even smaller than that of Ar^{2+} for the 2 Pa experiment, is well accounted for with this correction.

From a practical point of view, the heavy plasma ions (Ar^+, ArH^+) are especially relevant in sputtering processes. Budtz-Jørgensen et al.[2] have shown that the largest contribution to the physical sputtering of gold surfaces with Ar/H_2 DC discharges originates in the highly energetic ArH^+ ions. In this type of plasmas, symmetric charge exchange processes can lead to a significant reduction in the energy of the Ar^+ ions hitting the cathode (see for instance ref. 28 and references therein). The incorporation of H_2 to Ar plasmas, allowing the transformation of Ar^+ ions to ArH^+, was thus found to enhance ion sputtering. The present results indicate that in addition to the just mentioned energy loss, Ar^+ ions can be also neutralized in the sheath to a significant extent through asymmetric charge exchange with H_2 molecules. The light H_2^+ ions emerging from this process contribute much less to sputtering.

Summary and Conclusions

Cold plasmas formed in hollow cathode DC discharges of H_2/Ar (15%) have been experimentally investigated and modeled. The distributions of ion fluxes to the cathode and the electronic densities and temperatures in the negative glow of the plasma were determined using a mass spectrometer and a double Langmuir probe, respectively. The measurements were carried out at 2 Pa and 0.7 Pa. The ions identified at the two pressures were H^+, H_2^+, H_3^+, Ar^{2+}, Ar^+ and ArH^+, but the proportions of some of these ions varied markedly. In the lower

pressure discharge, the major ions, H_2^+ and H_3^+, were present in comparable amounts, whereas in the 2 Pa plasma, H_3^+ was neatly the dominant ionic species. The relative flux of Ar^+ ions hitting the cathode was found to decrease markedly with growing pressure. The measured electronic temperatures were 2.5 eV for 2 Pa and 3.5 eV for 0.7 Pa, these values are a factor of two lower than the corresponding temperatures for comparable plasmas of pure H_2

The experimental results have been analyzed by means of a simple zero-order kinetic model, which assumes homogeneous properties within the glow, and includes as input parameters the measured electron densities and the temperatures characterizing the assumed Maxwellian electron energy distributions. The measured electronic temperatures turned out to be too low to account for the observed ion-flux distributions and, notably, for the appearance of Ar^{2+}. The model was empirically corrected to include the contribution of a group of high energy (> 50 eV) "non Maxwellian" electrons. A small fraction (less than 3%) of these high energy electrons is enough to justify the experimental results. High energy electrons are found to be essentially responsible for the production of Ar^{2+} and are decisive for the explanation of the observed H_2^+/H_3^+ ratios. It is also found that a significant fraction of the Ar^+ ions formed in the plasma do not reach the cathode wall, but are transformed to neutral Ar through asymmetric charge exchange with H_2 molecules in the sheath. The attenuation of the Ar^+ flux to the cathode, which can be relevant for sputtering applications, can be satisfactorily modeled with a simple Lambert-Beer dependence using charge transfer cross sections from the literature.

ACKNOWLEDGEMENT

We are indebted to J. M Castillo, M. A. Moreno and J. Rodríguez for valuable technical assistance. This work has been funded by Ministry of Education of Spain under grants ENE2006-14577-C04, FIS2004-00456.

References

1 F. L. Tabarés and D. Tafalla, *J. Vac. Sci. Technol. A*, 1996, **14**, 3087.

2 C. V. Budtz- Jørgensen, P. Kringhøj, J. F. Nielsen and J. Bøttiger, *Surf. Coat. Technol.*, 1999, **116-119**, 938.

3 C. V. Budtz-Jørgensen, P. Kringhøj, J. F. Nielsen and J. Bøttiger, *Surf. Coat. Technol.*, 2001, **135**, 299.

4 N. Laidani, R. Bartali, P. Tosi and M. Anderle, *J. Phys. D: Appl. Phys*., 2004, **37**, 2593.

5 C. J. Rennick, R. Engeln, J. A. Smith, J. Orr-Ewing, N. M. R. Ashfold and Yu. A. Mankelevich, *J. Appl Phys*., 2005, **97**, 113306.

6 R. F. G. Meulenbroeks, A. J. Van Beck, A. J. G. Helvoort, M. C. M. Van de Sanden and D. C. Schram, *Phys. Rev. E.*, 1994, **49**, 4397.

7 R.F.G. Meulenbroeks, R. A. H. Engeln, M. N. A. Beurskens, R. M. J. Paffen, M. C. M. van de Sanden, J. A. M. van der Mullen and D. C. Schram, *Plasma Sources Sci. Technol.,* 1995, **4**, 74.

8 R.F.G. Meulenbroeks, D. C. Schram, M. C. M. van de Sanden and J. A. M. van der Mullen, *Phys. Rev. Lett.*, 1996, 76, 1840.

9 L. Thomas, J. L. Jauberteau, I. Jauberteau, J. Aubreton and A. Catherinot, *Plasma Chem. and Plasma Proc*., 1997, **17**, 193.

10 M. Kuraica, N. Konjevic, M. Platisa and D. Pantelic, *Spectrochim. Acta Part B*, 1992, **47**, 1173.

11 I. R. Videnovic, N. Konjevic and M. Kuraica, *Spechtrochimica Acta Part B*, 1996, **51**, 1707.

12 R. W. Smithwick III, D. W. Lynch and J. C. Franklin, *J. Am. Soc. Mass Spectrom*., 1993, **4**, 278.

13 M. Saito, *Anal. Chi. Acta*, 1997, **355**, 129.

14 V. D. Hodoroaba, V. Hoffmann, E. B. M. Steers and K. Wetzig, *J. Anal. At. Spectrom*., 2001, **15**, 1075.

15 E. B. M. Steers, P. Smid and Z. Weiss, *Spectrochim. Acta Part B*, 2006, **61**, 414.

16 K. Newman, R. S. Manson, D. R. Williams and I. P. Mortimer, *J. Anal. At. Spectrom*., 2004, **19**, 1192.

17 A. Menéndez, J. Pisonero, R. Pereiro, N. Bordel and A. Sanz-Medel, *J. Anal. At. Spectrom*., 2003, **18,** 557**.**

18 A. Martín, A. Menéndez, R. Pereiro, N. Bordel and A. Sanz-Medel, *Anal. Bional. Chem,* 2007, **388**, 1573.

19 T. G. Beuthe and J-S Chang, *Jpn. J. Appl. Phys.*, 1999, **38**, 4576.

20 R. Ye, T. Ishigaki, H. Taguchi, S. Ito, A. Murphy and H. Lange, *J. Appl. Phys*., 2006, **100**, 103303.

21 A. Bogaerts and R. Gijbels, *Phys. Rev. E*, 2002, **65**, 056402.

22 A. Bogaerts and R. Gijbels, *Spechtrochim. Acta Part B*, 2002, **57**, 1071.

23 A. Bogaerts, *J. Anal. At. Spectrom.,* 2008, **23**, 1441.

24 R. S. Mason, P. D. Miller and I. P. Mortimer, *Phys. Rev. E*, 1997, **55**, 7462.

25 I. Méndez, F. J. Gordillo-Vázquez, V. J. Herrero and I. Tanarro, *J. Phys. Chem. A*, 2006, **110**, 6060.

26 M. Castillo, I. Méndez, A. M. Islyaikin, V. J. Herrero and I. Tanarro, *J. Phys. Chem. A*, 2005, **109**, 6225.

27 V. J. Herrero, A. M. Islyiakin and I. Tanarro, *J. Mass Spectrom*., 2008, **43**, 1148.

28 I. Tanarro and V. J. Herrero, *Plasma Sources Sci. Technol*., 2009, **18**, 034007.

29 I. Tanarro, V. J. Herrero, A. M. Islyaikin, I. Méndez, F. L. Tabarés and D. Tafalla, *J. Phys. Chem. A*, 2007, **111**, 9003.

30 B. L. Schram, A. J. H. Boerboom, W. Kleine and J. Kistemaker, *Physica*, 1966, **32**, 749.

31 T. de los Arcos, C. Domingo, V. J. Herrero, M. M. Sanz, A. Schultz and I. Tanarro, *J. Phys. Chem. A*, 1998, **102**, 6282.

32 M. Castillo, V. J. Herrero and I. Tanarro, *Plasma Sources Sci. Technol*., 2002, **11**, 368.

33 V. G. Anicich, *J. Phys. Chem. Ref. Data,* 1993, **22**, 1469. JPL publication 03-19 NASA, 2003.

34 R. Rejoub, B. G. Lindsay and R. F. Stebbings, *Phys. Rev. A*, 2002, **65**, 042713.

35 R. D. Levine and R. B. Bernstein, *"Molecular Reaction Dynamics"*, Oxford University Press, New York, 1987, pp. 59-61.

36 B. A. Mitchell, O. Novotny, J. L. DeGarrec, A. Florescu-Mitchell, C. Rebrion-Rowe, A. V. Stolyarov, M. S. Child, A. Svendsen, M. A. El Ghazaly and L. H. Andersen, *J. Phys. B*, 2005, **38**, L175.

37 M. Larsson, B. J. McCall and A. E. Orel, *Chem. Phys. Lett.*, 2008, **462**, 145.

38 A. Bogaerts and Renaat Gijbels, *J. Appl. Phys.*, 1999, **86**, 4124.

39 K. F. Man, A. C. H. Smith and M. F. A. Harrison, *J. Phys. B*, 1987, **20**, 5865.

40 P. Gill and C. E. Webb, *J. Phys. D*, 1977, **10**, 299.

41 A. Bogaerts and R. Gijbels, *J. App. Phys.*, 1995, **78**, 2233.

42 J-S Yoon, M-Y Song, J-M Han, S. H. Hwang, W-S Chang, B-J Lee and Y. Itikawa, *J. Phys. Chem. Ref. Data*, 2008, **37**, 913.

43 K. M. Ervin and P. B. Armentrout, *J. Chem. Phys*., 1985, **83**, 166.

44 A. V. Phelps, *J. Phys. Chem. Ref. Data*, 1990, **19**, 653.

45 A. V. Phelps, *J. Chem. Phys. Ref. Dat*., 1992, **21**, 883.

46 A. V. Phelps, *J. Appl. Phys*., 1994, **76**, 747.

47 P. Franceschi, R. Thisen, O. Dutuit, C. Alcaraz, H. Soldi-Lose, D. Bassi, D. Ascenzi, P. Tosi, J. Zabka, Z. Herman, M. Coreno and M. De Simone, *Int. J. Mass Spectrom*., 2009, **280**, 119.

48 R. C. Amme and J. F. McIlwain, *J. Chem. Phys.*, 1966, **45**, 1224.